doi:10.1016/j.jmb.2009.08.053 J. Mol. Biol. (2009) 393, 735–752

JMB

Available online at www.sciencedirect.com

ScienceDirect

ELSEVIER

Characterization of the Heterogeneity and Specificity of Interpolypeptide Interactions in Amyloid Protofibrils by Measurement of Site-Specific Fluorescence Anisotropy Decay Kinetics

Anjali Jha[1], Jayant B. Udgaonkar[2]* and G. Krishnamoorthy[1]*

[1]*Department of Chemical Sciences, Tata Institute of Fundamental Research, Mumbai 400005, India*

[2]*National Centre for Biological Sciences, Tata Institute of Fundamental Research, Bangalore 560065, India*

Received 3 March 2009; received in revised form 24 July 2009; accepted 17 August 2009
Available online
28 August 2009

The aggregation of proteins often results in highly ordered fibrillar structures. While significant insights have been obtained on structural aspects of amyloid fibrils, little is known about the structures of protofibrils, which are presumed to be the precursors of fibrils. An understanding of the molecular mechanism of the formation of protofibrils and fibrils requires information on the landscape of interpeptide interactions. This work addresses this question by using, as a model protein, barstar, which forms protofibrils and fibrils at low (<3) pH. Use was made of the heterogeneity of aggregate populations encountered during fibril formation. Population heterogeneity was scored through rotational dynamics monitored by time-resolved fluorescence anisotropy of an environment-sensitive fluorophore, 5-((((2-iodoacetyl)amino)ethyl) amino)naphthalene-1-sulfonic acid (1,5-IAEDANS), attached to specific locations in the protein. Firstly, it was observed that barstar, when labeled at certain locations with 1,5-IAEDANS, did not form mixed protofibrils with the corresponding unlabeled protein. Labeled and unlabeled proteins formed protofibrils as separate populations. A two-population model of fluorescence anisotropy decay kinetics exhibiting a 'dip-and-rise' behavior was the main readout in arriving at this conclusion. Additional support for this conclusion came from the fluorescence lifetime of the probe 1,5-IAEDANS. Subsequently, the location of the fluorophore was moved along the length of the protein in nine mutant proteins, and the capability to form mixed fibrils was assessed. The results revealed that about two-thirds of the protein sequence at the C-terminal end of the protein was intimately involved in the formation of ordered protofibrils, probably forming the core, while the remaining one-third of the protein (i.e., the N-terminal region) remained largely noninteractive and flexible. This methodology can be used as a general strategy to identify regions of a given protein sequence involved in interprotein interactions in amyloid protofibrils.

Keywords: barstar; amyloid protofibrils; time-resolved fluorescence anisotropy decay; two-population anisotropy decay; interpeptide interactions

Edited by J. Weissman

Introduction

Deposits or accumulations of aggregated proteins are one of the hallmarks of many neurodegenerative diseases.[1–5] These deposits are formed by thread-like structures,[6] which are usually referred to as amyloid or amyloid-like fibrils. Recent studies have suggested that the main toxicity of amyloidogenic proteins lies in the spherical oligomers and

**Corresponding authors.* E-mail addresses: jayant@ncbs.res.in; gk@tifr.res.in.

Abbreviations used: 1,5-IAEDANS, 5-((((2-iodoacetyl) amino)ethyl)amino)naphthalene-1-sulfonic acid; AFM, atomic force microscopy; ThT, thioflavin T; IRF, instrument response function.

the small wormlike protofibril intermediates, which form early during the protein aggregation process, rather than in the insoluble, more straight fibrils that accumulate in tissues.[7–10] Understanding the mechanism of the conformational change by which functional proteins transform into soluble aggregates that are toxic, such as the spherical oligomers and elongated protofibrils, is therefore important for designing therapies for the treatment of neurodegenerative diseases. However, in contrast to the availability of structural information on amyloid fibrils,[11–15] there is a dearth of knowledge on the internal structures of soluble aggregates and protofibrils.

Fluorescence-based methods have been shown to be powerful in the structural characterization of protofibrils and fibrils.[16–20] Fluorescence has the advantage of being a highly sensitive technique capable of providing residue-specific information. Furthermore, time-domain fluorescence has the capability of addressing the question of heterogeneity in a given population of protein aggregates, unlike several other techniques such as NMR, which provide only ensemble-averaged information. This is because interconversion of various conformations is usually slow when compared to the nanosecond timescale of fluorescence lifetimes. Residue-specific fluorescence anisotropy measurements have been particularly effective in showing that the soluble oligomers of barstar transform directly into protofibrils without undergoing drastic structural rearrangements.[20]

The ability of proteins to form amyloid-like fibrils is not restricted only to amyloidogenic proteins associated with diseases. Many other proteins and peptides also form amyloid like-fibrils *in vitro* under well-defined conditions of pH, temperature, and ionic strength.[21–23] Thus, protein aggregation depends not only on the polypeptide sequence but also on external conditions. This provides an opportunity to study the structural characteristics of aggregates and fibrils by using a model protein such as barstar. Barstar, an 89-residue protein with no disulfide bond, is the intracellular inhibitor of the extracellular ribonuclease barnase in *Bacillus amyloliquefaciens*, and its folding–unfolding reactions have been well characterized.[24–27] The three-dimensional solution structure of barstar is known from NMR studies[28] and is composed of three α-helices (residues 14–25, 33–43, and 68–81) packed against a three-stranded parallel β-sheet (residues 1–6, 49–54, and 83–89). A more poorly defined helix (residues 56–63) links the second β-strand to the fourth α-helix (Fig. 1).

Barstar forms soluble aggregates (the A-form) at pH<3, which have been studied by NMR and characterized as 160-kDa molten globule-like structures.[29] Circular dichroism (CD) and time-resolved fluorescence studies have shown that the A-form does not possess any tertiary structure, whereas secondary structures remain partially unperturbed.[30,31] The A-form transforms into protofibrils in a slow process that is accelerated at higher temperature.[20,32–34] The details of the internal arrangement of individual polypeptides and their interactions with neighboring polypeptides in the protofibrils are unknown.

In this work, the heterogeneity of the aggregated sample and the specificity of interpolypeptide interactions in amyloid protofibrils of barstar have been

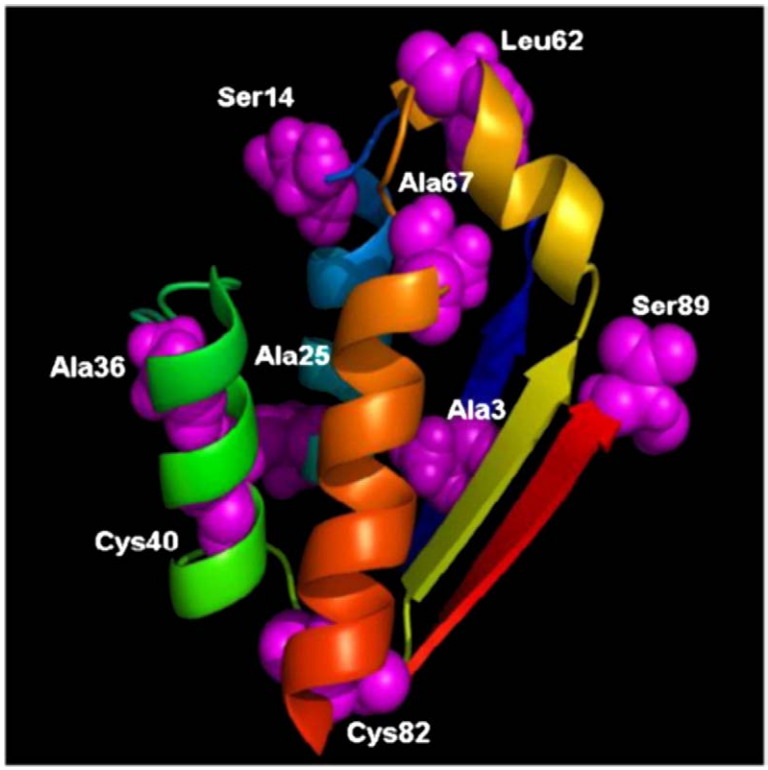

Fig. 1. Structure of barstar. The locations of the nine different residues that were mutated to cysteine are shown. The structure was drawn using PyMOL and the Protein Data Bank file 1A19.

probed by time-resolved fluorescence spectroscopy. Nine single cysteine-containing mutant forms of barstar (Fig. 1) have been studied.[35] The selected residue positions (3, 14, 25, 36, 40, 62, 67, 82, and 89) scan the entire length of the protein. The proteins were labeled with a thiol-labeling fluorescence probe, 5-((((2-iodoacetyl)amino)ethyl)amino)naphthalene-1-sulfonic acid (1,5-IAEDANS). The site-specific fluorescence intensity decay kinetics, as well as the anisotropy decay kinetics of mixtures of labeled and unlabeled proteins, were monitored to probe whether the entire length of the protein is involved in forming protofibrils or whether some segments remain flexible, while others form the ordered core. The results show that the C-terminal two-thirds of the protein sequence is involved in self-complimentary interaction in the protofibril core, while the N-terminal one-third of the sequence remains largely noninteractive and flexible. Very interestingly, a labeled protein and the corresponding unlabeled protein do not form mixed protofibrils, when the label is present in the C-terminal region corresponding to the core of the amyloid protofibrils.

Results

Population heterogeneity probed by rotational dynamics

Protein aggregation is known to be heterogeneous in nature, resulting in the formation of a wide variety of structures of different size and morphology. The structural polymorphism has been studied in detail in some proteins.[36–39] In this work, measurement of this heterogeneity is used as a probe to check whether two proteins differing only at a single site can co-aggregate and form mixed protofibrils. Measurement of the hydrodynamic radii of the constituents of a population of protein aggregates is a direct method to probe the structural heterogeneity of the product of aggregation. Fluorescence anisotropy is a sensitive tool to estimate the hydrodynamic radius of a macromolecule, as rotational diffusion, which causes fluorescence depolarization, scales with the volume of the macromolecule.

The kinetics of formation of protofibrils from the A-form of barstar depend on the protein concentration. At lower protein concentrations (<5 μM), the rate of aggregation is very slow, but the kinetics remain single exponential with no lag phase, when the protein concentration is varied in the range of 1 to 50 μM.[32,34] The process of protofibril formation occurs in steps that involve progressively higher oligomeric intermediates.[32,34] Hence, at low protein concentrations, a high level of structural heterogeneity in the aggregated product can be expected, and oligomeric intermediates of different sizes will be present. The fluorescence anisotropy decay kinetics of the products of the aggregation of 2 and 50 μM barstar covalently labeled with 1,5-IAEDANS at C82 of the single cysteine-containing mutant form Cys82 of the protein are shown in Fig. 2. It can be seen that the decay kinetics are remarkably different for the two different protein concentrations. While the high-concentration (50 μM) sample shows an apparently normal behavior of the anisotropy decay kinetics, the low-concentration (2 μM) sample shows

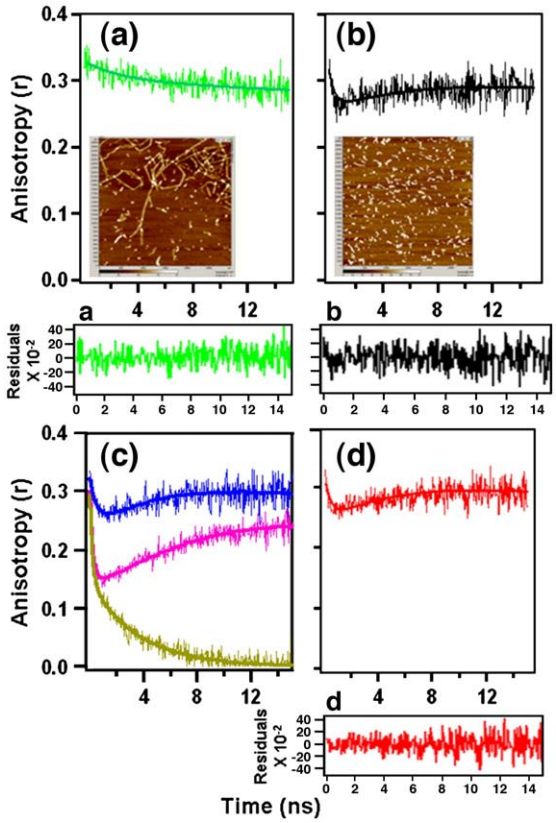

Fig. 2. Concentration-dependent anisotropy decay kinetics of the protofibrils formed by Cys82-IAEDANS. (a) shows the time-resolved anisotropy decay curve of the protofibrils formed by 50 μM Cys82-IAEDANS and (b) shows the time-resolved anisotropy decay curve of the protofibrils formed by 2 μM Cys82-IAEDANS. (c) shows the fluorescence anisotropy decay kinetics during the aggregation of 2 μM Cys82-IAEDANS at 5 min (dark yellow line), 35 min (pink line), and 2.5 h (blue line) of heating. The smooth lines shown in this panel are the fits generated to Eqs. (5)–(9) and the fraction of population 1 obtained is ~1.0, 0.65, and 0.3 for 5 min, 35 min, and 2.5 h, respectively, of heating at 70 °C. (d) shows the time-resolved anisotropy decay curve of the protofibrils obtained from a mixture of 2 μM of the IAEDANS-labeled and 48 μM of unlabeled Cys82. For (a), (b), and (d), the smooth lines are the fits generated to Eqs. (2)–(9), and the parameters are listed in Table 1. The insets show the AFM images (taken in liquid medium) of the protofibrils formed from either the 50 μM sample (a) or the 2 μM sample (b). The final concentration of the protein was kept identical in both of the liquid-phase (50 mM glycine, pH 2.7) AFM images. (a), (b), and (d) show the residuals of the fitting of anisotropy decay kinetics shown in (a), (b) and (d), respectively. Also, the χ^2 values of the three fittings are 1.05, 1.11, and 1.01, respectively.

a 'dip-and-rise' behavior. This is a hallmark of the presence of at least two populations, one with a short fluorescence lifetime and a short rotational correlation time and another having both the time constants significantly longer compared to those of the first population.[39–42] Atomic force microscopy (AFM) images of the two samples imaged under liquid conditions (Fig. 2, inset) show that while the 50 μM sample consists mainly of protofibrils or higher oligomers, the 2 μM sample shows the presence of only smaller oligomers. Based on these data, it appears that the product of aggregation of the 50 μM sample consists of protofibrils and higher oligomers (as seen in the AFM image) giving rise to anisotropy decay kinetics (Fig. 2a), which can be fitted to a sum of two correlation times ($\varphi_1 = 2.0$ ns and $\varphi_2 > 100$ ns), representing the local and global rotational dynamics of the covalently attached (1,5-IAEDANS) label.[20] The limiting value of $\varphi_2 > 100$ ns comes from the finite time window offered by the fluorescence lifetime of 1,5-IAEDANS. For the 2 μM sample, it appears that a combination of very small and larger oligomeric intermediates gives rise to the observed dip-and-rise anisotropy decay kinetics (Fig. 2b) because of the significant differences in the fluorescence lifetimes and rotational correlation times of the two populations. Such a dip-and-rise behavior has been observed previously in several situations[41] including protein aggregation.[39] Figure 2 also shows the fits to the anisotropy decay kinetics of both the high- and low-concentration samples, based on a two-population model [see Model used and data analysis; Eqs. (2)–(9)]. The values of the parameters obtained from the fits are given in Table 1. It is seen that for the two populations (very small and larger oligomeric intermediates) proposed for the 2 μM sample, the values of the fluorescence parameters are such as to give rise to dip-and-rise fluorescence anisotropy decay kinetics; one population is characterized by having both the lifetimes and correlations times significantly shorter than those of the other population. The population labeled as very small oligomers could well be monomers, as judged by their single rotational correlation time of 0.4 ns (population 1 in Table 1). A two-population model was used in fitting the dip-and-rise anisotropy decay kinetics because it is the simplest model that can account fully for the data. The observation that a two-population model can adequately describe the data suggests that, although much more structural heterogeneity may be present, the molecules can yet be classified into two populations in terms of their fluorescence properties. It is fortunate in this case that the two-population model can adequately describe the data. The use of models with more than two populations would require many more free parameters to fit the data, and it may have been difficult to obtain reliable values for the larger number of parameters required to describe more complex models, given the S/N ratio of the data.

Figure 2c shows the time evolution of the dip-and-rise pattern of the fluorescence anisotropy decay

Table 1. Parameters associated with the fluorescence anisotropy decay kinetics of protofibrils formed from 1,5-IAEDANS-labeled Cys82

		Population 1			Population 2			
		Fluorescence lifetimes (amplitudes)		Rotational correlation time	Fluorescence lifetimes (amplitudes)		Rotational correlation times (amplitudes)	
Sample	Fraction of population 1	τ_{11} [ns] (α_{11})	τ_{12} [ns] (α_{12})	ϕ_{11} [ns]	τ_{21} [ns] (α_{21})	τ_{22} [ns] (α_{22})	ϕ_{21} [ns] (β_{21})	ϕ_{22} [ns] (β_{22})
50 μM of labeled protein	—	—	—	—	7.0±0.7 (0.15±0.01)	20±2 (0.85±0.02)	2.0±0.2 (0.07±0.02)	>100 (0.93±0.03)
2 μM of labeled protein	0.30±0.01	5.3±0.2 (0.50±0.01)	0.47±0.02 (0.50±0.02)	0.45±0.01	7.5±0.4 (0.44±0.02)	22±2 (0.56±0.03)	0.98±0.09 (0.10±0.02)	>100 (0.90±0.02)
Mixture of 2 μM labeled and 48 μM unlabeled proteins	0.30±0.01	2.9±0.5 (0.51±0.01)	0.58±0.03 (0.49±0.01)	0.44±0.01	7.1±0.7 (0.38±0.03)	22±3 (0.62±0.03)	0.99±0.05 (0.10±0.03)	>100 (0.90±0.02)

Fluorescence anisotropy decay kinetics were analyzed using Eqs. (4) and (5).

Table 2. Fluorescence lifetimes and their amplitudes in protofibrils of 1,5-IAEDANS-labeled Cys82 at two different concentrations, upon excitation at three different wavelengths

Concentration	Excitation wavelength, λ_{ex} [nm]	Fluorescence lifetimes (amplitudes)			Mean fluorescence lifetime, τ_m [ns]
		τ_1 [ns] (α_1)	τ_2 [ns] (α_2)	τ_3 [ns] (α_3)	
2 μM of IAEDANS-labeled protofibrils	410	18.1 (0.60)	4.2 (0.15)	0.92 (0.25)	11.7
	390	18.0 (0.80)	5.8 (0.15)	0.56 (0.05)	15.3
	370	18.2 (0.88)	6.5 (0.12)	—	16.8
50 μM of IAEDANS-labeled protofibrils	410	19.0 (0.89)	7.9 (0.11)	—	17.7
	390	18.5 (0.92)	11.7 (0.08)	—	17.9
	370	18.1 (1.0)	—	—	18.1

Mean fluorescence lifetime $\tau_m = \sum \alpha_i \tau_i$. The error associated with the fluorescence lifetime measurement (τ) and its amplitude (β) is <10%.

kinetics, during the aggregation of 2 μM protein at 70 °C. At early times of aggregation, only population 1 is observed. Population 2 is observed to increase with the time of aggregation at the expense of population 1. This indicates that the small oligomers or monomers in population 1 grow over time to become the higher oligomers or protofibrils in population 2.

The enhanced level of heterogeneity of population in the product of aggregation of the 2 μM sample when compared to that of the 50 μM sample can also inferred from the fluorescence lifetimes of the products of the aggregation of the two samples (Table 2, 410 nm excitation). While the 50 μM sample shows nearly single exponential behavior (with a minor second component of <12% amplitude), the 2 μM sample shows large heterogeneity with three time constants having significant amplitudes. The mean lifetime (τ_m) of the 2 μM sample is significantly smaller when compared to that of the 50 μM sample (see the excitation wavelength dependence below).

Probing the interaction between unlabeled and fluorescently labeled proteins

The observations presented in the previous section enable addressing the question whether unlabeled and fluorescently labeled barstar molecules aggregate together and form mixed fibrils. The mixing of the 2 μM sample labeled with 1,5-IAEDANS at C82 with the 48 μM unlabeled sample, prior to commencement of the aggregation process, can be expected to result in one of the following two alternative scenarios: (i) the labeled and unlabeled proteins interact with each other and form mixed fibrils, and (ii) the two proteins form their own individual aggregates, without interacting with each other. Based on the observations shown in Fig. 2, the behavior shown in Fig. 2a is expected for the former scenario and that in Fig. 2b is expected for the latter. This is because the mixed fibrils, if formed, will have rotational dynamics very similar to that of the 50 μM sample (Fig. 2a) in spite of the low levels of fluorescence labeling (namely, 1 in 25 protein molecules will be labeled in every protofibril formed). Thus, the rotational dynamics becomes the window to answer the interesting question related to the capability to form mixed fibrils.

Figure 2d shows the results of the mixing experiment outlined above. It is clear that the two samples used here do not interact with each other and do not form mixed protofibrils as the anisotropy decay kinetics of the 'mixed' sample (2 μM of labeled + 48 μM of unlabeled) is nearly identical with that of the 2 μM sample. The analysis of the anisotropy decay kinetics was carried out using Eqs. (5)–(9) (Table 1). The rotational correlation time obtained for the mixed sample is closer to that of the 2 μM sample, indicating that the labeled and unlabeled proteins do not interact with each other. These results can be interpreted as indicating that position 82 is involved intimately in self-complimentary interactions when protein molecules form the protofibril, and attaching a fluorescence label at that location perturbs the self-complimentary interactions.

It should be noted that the question of mixed fibril formation could be addressed mainly due to the sensitivity of the dansyl fluorophore (1,5-IAEDANS) used in the experiments[43] and also to the selection of wavelengths used for excitation and emission of the fluorophore. The fluorescence lifetime of protein-coupled 1,5-IAEDANS is quite sensitive to the environment. The fluorescence lifetime of the 2 μM aggregated sample is significantly smaller than that of the 50 μM sample (Table 2). This is essential to produce the observed dip-and-rise anisotropy decays.[42] Furthermore, both the anisotropy decay kinetics and fluorescence lifetime depend upon the excitation wavelength used, especially for the 2 μM aggregated sample (Table 2 and Fig. 3a), in which the population is expected to be quite heterogeneous. It can be seen that the dip-and-rise pattern in the anisotropy decay is seen only upon excitation at 410 nm but not upon excitation at other wavelengths such as 370 or 390 nm (Fig. 3a). In contrast, the 50 μM aggregated sample does not show any significant dependence on the excitation wavelength, either in the lifetime or in the anisotropy decay kinetics (Table 2 and Fig. 3b). In order to resolve these perplexing data, the fluorescence excitation spectrum of the aggregated sample was measured at various protein concentrations and found to be concentration dependent: at lower

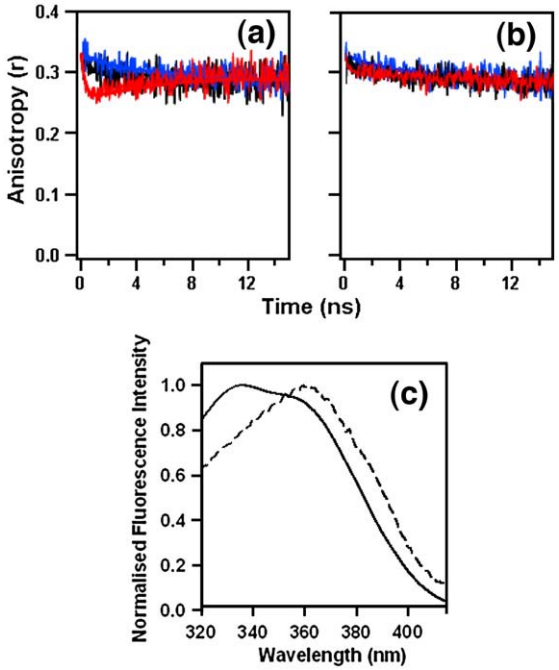

Fig. 3. Dependence of the fluorescence anisotropy decay kinetics on the excitation wavelength. (a) and (b) show the time-resolved anisotropy decay kinetics of protofibrils produced by 2 and 50 μM Cys82-IAEDANS, respectively, upon excitation at 370 nm (black line), 390 nm (blue line), and 410 nm (red line) wavelengths. The smooth lines are the fits to Eq. (5) (a) and to Eq. (4) (b). (c) shows normalized excitation spectra of the protofibrils formed by 0.05 μM (broken line) and 50 μM (continuous line) Cys82-IAEDANS, while the emission was monitored at 525 nm.

concentrations, a red shift in the excitation spectrum is seen (Fig. 3c). Based on these observations, it is hypothesized that the 50 μM sample is fairly homogeneous (as far as fluorescence decay parameters are concerned), resulting in the excitation wavelength independence of the anisotropy decay kinetics (Fig. 3b) and fluorescence lifetimes (Table 2), and that the 2 μM sample is heterogeneous, resulting in the excitation wavelength dependence of both these observables (Fig. 3a and Table 2). It appears that the heterogeneity in the 2 μM sample is such that it has at least two populations: one whose excitation spectrum is red shifted compared to that of the homogeneous population seen in the case of the 50 μM sample (Fig. 3c) and the other whose excitation spectrum is similar to that of the 50 μM sample. The former population, which is different from the homogeneous population in the 50 μM sample, appears to consist of very small oligomers on the basis of the measurement of the single rotational correlation time of 0.4 ns (Table 1). Thus, excitation towards the red side of the excitation spectra results in capturing the relatively large fraction of the first population and leads to the prominent dip-and-rise anisotropy decay kinetics (red trace in Fig. 3a).

Identification of sites involved in the formation of protofibrils of barstar

The internal structure of polypeptides in amyloid protofibrils is largely unknown at the individual residue level. Since the entire length of a protein molecule need not be incorporated in the ordered core structure of the protofibrils, the residues involved in the compact core structure need to be identified. In this study, the strategy used to locate the residues that constitute the ordered core of protofibrils is based on the experiment outlined in the previous section, viz., comparison of the fluorescence anisotropy decay kinetics and fluorescence lifetimes of the protofibrils formed by the mixed sample (2 μM of protein labeled at a specific location + 48 μM of unlabeled protein) with those of the individual 2 and 50 μM samples, labeled at the same location. If the mixed sample shows anisotropy and intensity decay kinetics similar to that of the 2 μM sample, it is taken as an indication of the absence of the formation of mixed protofibrils, as observed in the case of Cys82. Conversely, if the mixed sample shows fluorescence characteristics similar to those of the 50 μM sample, it is taken to indicate that the labeled and unlabeled proteins interact with each other, resulting in the formation of mixed protofibrils.

Nine single cysteine-containing mutant forms of barstar were made and probed by the method outlined above. Figure 4 shows the fluorescence anisotropy decay kinetics of the nine 1,5-IAEDANS-labeled single cysteine mutant forms of barstar. Each panel shows the data for 2 μM, 50 μM, and the mixed samples. The results show the following: for the first three mutant proteins (Cys3, Cys14, and Cys25), the mixed sample behaves similar to the 50 μM sample, while for the other mutant proteins (Cys36, Cys40, Cys62, Cys67, Cys82, and Cys89), the mixed sample has kinetics similar to that of the 2 μM sample. Similar behavior is also seen for the fluorescence lifetimes (Table 3). The mixed samples have fluorescence decay kinetics very similar to that of the 50 μM sample for Cys3, Cys14, and Cys25 and to that of the 2 μM sample for the other mutant proteins. These results indicate that the protein labeled with the fluorophore in the N-terminal one-third of the entire sequence (residues ~1–30) can form mixed protofibrils with unlabeled protein. In contrast, when the label is located in the remaining two-thirds of the sequence (residues ~30–89) of the protein, the formation of mixed protofibrils does not occur.

Site-specific dynamics in protofibrils

The fluorescence anisotropy decay curves for the protofibrils formed by 50 μM protein labeled at various locations are found to be quite similar in terms of their kinetics with some small differences (Table 4). For all the mutant proteins, the decay kinetics can be fitted to a model with two rotational correlation times [Eq. (4)], namely, a fast component

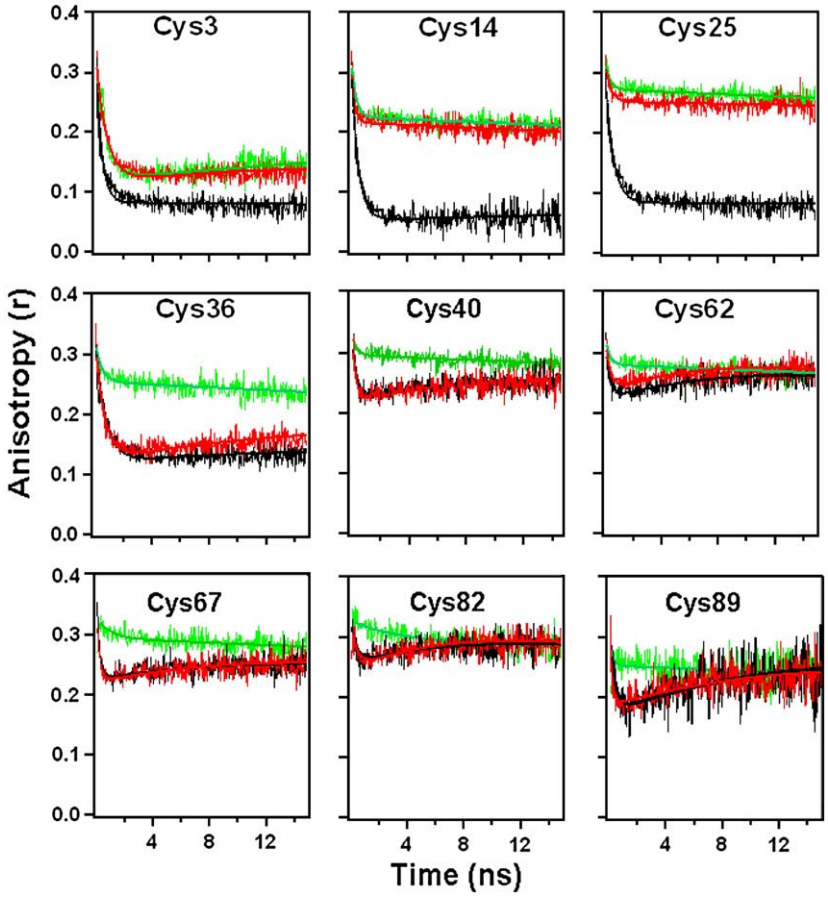

Fig. 4. Fluorescence anisotropy decay kinetics of the fluorophore in the protofibrils formed from the nine different mutant proteins at different concentrations. Each panel shows the anisotropy decay kinetics for the protofibrils formed by 50 μM of the labeled protein (green line), 2 μM of the labeled protein (black line), and a mixture of 2 μM of the labeled protein and 48 μM of the unlabeled protein (red line). The smooth lines are the fits to Eqs. (2)–(9), and the parameters are listed in Tables 3–6.

(ϕ_1<2 ns) and a very long component with ϕ_2>100 ns as described above. While the first component can be assigned to rapid local motion of the fluorescence probe with respect to the macromolecule, the longer component appears to be due to the slow tumbling motion of fibrils. The amplitude associated with the local motion (β_1) shows significant variation along the length of the polypeptide. In our earlier work,[20] this variation had been interpreted as representing a 'dynamic map' of the polypeptide structure in the fibril. The observation of significantly higher values of β_1 for residues in the N-terminal region when compared to other residues (Table 4) had indicated that the N-terminal region is more flexible and that the core structure of the fibril is formed by the major part of the C-terminal region of the protein.

The fluorescence anisotropy decay kinetics of protofibrils formed by 2 μM labeled mutant proteins were analyzed using a two-population model [Eq. (5)] as in the case of the Cys82 protein described above. The parameters obtained from the fits to the data are listed in Table 5. The fraction of the first population (very small oligomers) is seen to be ~30–45%. This population is associated with a single rotational correlation time ϕ_m<1 ns, which is also seen in denatured monomers of barstar.[44] The rotational dynamics of the second population (larger oligomeric intermediates) were fitted to a sum of two correlation times, as described earlier, for all the mutant proteins. The correlation times and their amplitudes are very similar to those obtained for the 50 μM sample. Interestingly, site-dependent differences are observed in the dynamics of the second population. Residues close to the N-terminus (C3, C14, C25, and C36) show longer rotational correlation times of ~40 ns, whereas for the other residues (C89, C82, C67, C62, and C40), the longer correlation time is >100 ns, the value limited by the fluorescence observation window. This indicates that the N-terminal region is flexible and that the C-terminal region is more compact even in the larger oligomeric intermediates (population 2) formed in the 2 μM sample.

Analysis of the fluorescence anisotropy decay kinetics of the protofibrils formed from the mixed (mixture of 2 μM of labeled and 48 μM of unlabeled proteins) samples of all the mutant proteins was also carried out by using the two-population model, as in the case of the 2 μM labeled proteins. The results given in Table 6 indicate that the protofibrils formed by the C-terminal region mutant proteins Cys36, Cys40, Cys62, Cys67, Cys82, and Cys89 show the fraction of population 1 to be ~30–45%, which is similar to that obtained with 2 μM of the labeled mutant proteins alone. In contrast, this fraction diminishes significantly (to ~10%) for the N-terminal region mutant proteins Cys3, Cys14, and Cys25. This is in line with the earlier conclusion that the protein labeled at the N-terminal residues

Table 3. Fluorescence lifetimes and their amplitudes in protofibrils of all the nine mutant proteins labeled with 1,5-IAEDANS at different concentrations

Proteins	Concentration	Fluorescence lifetimes (amplitudes) τ_1 [ns] (α_1)	τ_2 [ns] (α_2)	τ_3 [ns] (α_3)	Mean fluorescence lifetime, τ_m [ns]
Cys3	50 μM	19.9 (0.71)	8.4 (0.19)	0.80 (0.10)	15.9
	2 μM	14.7 (0.67)	7.0 (0.20)	0.77 (0.12)	11.4
	Mix	18.5 (0.81)	3.7 (0.09)	0.30 (0.10)	15.4
Cys14	50 μM	19.9 (0.72)	8.4 (0.18)	0.85 (0.10)	15.9
	2 μM	13.4 (0.72)	9.1 (0.26)	0.43 (0.02)	12.0
	Mix	18.6 (0.84)	4.0 (0.07)	0.80 (0.09)	16.0
Cys25	50 μM	17.4 (0.98)	5.4 (0.02)	—	17.2
	2 μM	13.2 (0.79)	8.5 (0.19)	0.50 (0.02)	12.0
	Mix	20.4 (0.68)	11.2 (0.21)	1.40 (0.10)	16.5
Cys36	50 μM	18.5 (0.83)	3.6 (0.09)	0.38 (0.08)	15.8
	2 μM	18.0 (0.58)	3.8 (0.26)	0.34 (0.16)	11.5
	Mix	17.8 (0.66)	4.1 (0.20)	1.30 (0.14)	12.8
Cys40	50 μM	18.0 (0.80)	10.0 (0.20)	—	17.2
	2 μM	13.4 (0.72)	9.2 (0.26)	0.43 (0.02)	12.0
	Mix	13.3 (0.69)	10.2 (0.30)	2.50 (0.01)	12.2
Cys62	50 μM	18.7 (0.80)	10.5 (0.20)	—	17.0
	2 μM	13.2 (0.69)	10.3 (0.30)	2.50 (0.01)	12.2
	Mix	18.8 (0.67)	2.9 (0.14)	0.50 (0.19)	13.1
Cys67	50 μM	18.8 (0.90)	7.7 (0.10)	—	16.9
	2 μM	13.4 (0.72)	9.1 (0.26)	0.43 (0.02)	12.0
	Mix	18.5 (0.57)	4.7 (0.26)	0.55 (0.17)	11.8
Cys82	50 μM	19.0 (0.88)	7.4 (0.12)	—	17.6
	2 μM	17.9 (0.58)	4.3 (0.18)	0.95 (0.24)	11.4
	Mix	19.0 (0.53)	3.9 (0.19)	0.70 (0.28)	11.1
Cys89	50 μM	17.2 (1.0)	—	—	17.2
	2 μM	19.4 (0.63)	3.2 (0.19)	0.60 (0.18)	12.9
	Mix	19.3 (0.62)	2.8 (0.20)	0.50 (0.18)	12.6

'Mix' refers to the mixture of 2 μM labeled and 48 μM unlabeled proteins.
Errors are not mentioned explicitly in order to improve clarity. Errors are ~10%.

can co-aggregate with the corresponding unlabeled proteins, leading to the formation of nearly a single population. The rotational dynamics of the second population (population 2) in the mixed sample (Table 6) shows interesting differences from the dynamics of the 2 μM labeled sample (Table 5). The longer correlation time of this population for the protofibrils formed by proteins labeled at C3, C14, and C25 is >100 ns (Table 6), similar in value to the long correlation times obtained with the labeled mutant protein at other positions but in contrast to the observations made in the case of the 2 μM samples, which had values of ~40–50 ns (Table 5). Once again, this observation is taken to indicate the formation of mixed fibrils between unlabeled and labeled mutant proteins with the label in the N-terminal region (Cys3, Cys14, and Cys25). In the case of other residue positions, the parameters obtained in the analysis are very similar for the 2 μM and the mixed samples (Tables 5 and 6), once again reinforcing the interpretation that proteins labeled at these positions do not form mixed protofibrils with the corresponding unlabeled mutant proteins.

Table 4. Rotational correlation times (ϕ) and their amplitudes (β) in protofibrils of all the nine mutant proteins labeled with 1,5-IAEDANS

Proteins	ϕ_1 [ns] (β_1)	ϕ_2 [ns] (β_2)
Cys3	0.4 (0.39)	>100 (0.61)
Cys14	1.1 (0.20)	>100 (0.80)
Cys25	1.0 (0.13)	>100 (0.87)
Cys36	0.6 (0.15)	>100 (0.85)
Cys40	1.5 (0.10)	>100 (0.90)
Cys62	0.6 (0.12)	>100 (0.88)
Cys67	1.2 (0.09)	>100 (0.91)
Cys82	2.0 (0.07)	>100 (0.93)
Cys89	1.6 (0.12)	>100 (0.88)

The concentration of the proteins was 50 μM. Fluorescence anisotropy decay kinetics were analyzed using Eqs. (2)–(4).
The error in β_1 and β_2 is ~0.03; in ϕ_1, the error is <0.2.

It should be pointed out that the absence of the dip-and-rise behavior in the fluorescence anisotropy decay by itself cannot be used to rule out the presence of two (or more) populations. The manifestation of a dip-and-rise pattern depends on the parameters associated with the decay kinetics of the fluorescence intensity and anisotropy of the two populations.[45]

Fluorescence labeling does not perturb the aggregation property of the polypeptide

In order to address the question whether fluorescence labeling by 1,5-IAEDANS perturbs the aggregation property of barstar, the kinetics of formation of fibrils by two different labeled mutant proteins were studied using the thioflavin T (ThT) assay as described earlier.[32,34] Two mutant proteins, namely, Cys3 and Cys82, were selected for the study of aggregation kinetics. Figure 5 shows the kinetics of formation of amyloid protofibrils at 70 °C from 1,5-

Table 5. Rotational correlation times (ϕ) and their amplitudes (β) in protofibrils formed by all the nine mutant proteins labeled with 1,5-IAEDANS

	Population 1				Population 2			
		Fluorescence lifetimes (amplitudes)		Rotational correlation time	Fluorescence lifetimes (amplitudes)		Rotational correlation times (amplitudes)	
Proteins	Fraction of population 1	τ_{11} [ns] (α_{11})	τ_{12} [ns] (α_{12})	ϕ_{11} [ns]	τ_{21} [ns] (α_{21})	τ_{22} [ns] (α_{22})	ϕ_{21} [ns] (β_{21})	ϕ_{22} [ns] (β_{22})
Cys3	0.32	6.6 (0.85)	0.50 (0.15)	0.80	9.6 (0.25)	22.7 (0.75)	1.8 (0.10)	42 (0.90)
Cys14	0.30	6.0 (0.83)	0.30 (0.17)	0.75	8.0 (0.20)	20 (0.80)	2.0 (0.10)	40 (0.90)
Cys25	0.32	6.5 (0.80)	0.40 (0.20)	0.70	8.5 (0.21)	22 (0.79)	2.0 (0.12)	45 (0.88)
Cys36	0.35	7.5 (0.85)	0.28 (0.15)	0.70	11.9 (0.30)	23 (0.70)	2.2 (0.10)	57 (0.90)
Cys40	0.29	4.5 (0.60)	0.70 (0.40)	0.53	7.3 (0.30)	22 (0.70)	2.3 (0.13)	>100 (0.87)
Cys62	0.30	7.2 (0.64)	0.69 (0.36)	0.50	7.0 (0.44)	29 (0.56)	1.1 (0.10)	>100 (0.90)
Cys67	0.32	7.0 (0.63)	0.60 (0.36)	0.40	7.6 (0.45)	29 (0.55)	1.0 (0.10)	>100 (0.90)
Cys82	0.30	5.2 (0.50)	0.45 (0.50)	0.46	7.6 (0.43)	23 (0.57)	0.98 (0.10)	>100 (0.90)
Cys89	0.35	4.6 (0.52)	0.32 (0.48)	0.30	6.0 (0.50)	20 (0.50)	0.8 (0.09)	>100 (0.91)

The concentration of the proteins was 2 μM. Fluorescence anisotropy decay kinetics were analyzed using Eqs. (5)–(9).
Errors are not mentioned explicitly in order to improve clarity. Errors associated with each measurement are <10%.

IAEDANS-labeled and unlabeled Cys3 and Cys82, monitored by the increase in ThT fluorescence at 482 nm. It is seen that the rate constants associated with the increase in fluorescence intensity, described by single exponentials, do not depend significantly on fluorescence labeling for both the mutant proteins. Thus, the result indicates that the labeling does not significantly perturb the rate constant of aggregation.

CD is an important tool to probe the secondary-structure content of polypeptides in various structural forms, including protein fibrils. It was important to ask whether labeling by 1,5-IAEDANS alters the internal structure of the protofibrils as probed by CD. Far-UV CD spectra obtained for the two mutant proteins Cys3 and Cys82, one each from the two regions identified from the studies elaborated above, are shown in Fig. 6. The following observations can be made: (i) The CD spectra of both the unlabeled proteins (Cys3 and Cys82) are very similar to each other, for both the A-form (Fig. 6a) and the protofibril form (Fig. 6c). (ii) The CD spectra of the protofibrils show a higher content of β-sheet compared to those of the A-form (compare Fig. 6a and c). (iii) The CD spectrum of the A-form formed by unlabeled Cys82 (Fig. 6a) is entirely different from that formed from labeled Cys82 (Fig. 6b). The same extent of difference between the unlabeled and labeled Cys82 is seen for the protofibrils also (Fig. 6c and d), which suggests that labeling at C82 affects the secondary structure in both the A-form and protofibrils. Earlier studies had shown that the A-form is the precursor of protofibrils.[20] Thus, the results suggest that any perturbation of structure in the protofibrils by labeling might originate from perturbation of the A-form structure. (iv) In contrast, for Cys3, the labeled and unlabeled proteins show similar secondary structures, in the A-form as well as in the protofibril form. These results indicate that the labeling perturbs the internal secondary structure of the A-form, as well as of the protofibrils, only in the case of Cys82. This last observation may be related to the observation that C82 is most likely involved in making intermolecular contacts while forming the aggregate as opposed to Cys3. The different behaviors of the two mutant proteins

Table 6. Rotational correlation times (ϕ) and their amplitudes (β) in protofibrils formed by all the nine mutant proteins labeled with 1,5-IAEDANS

	Population 1				Population 2			
		Fluorescence lifetimes (amplitudes)		Rotational correlation time	Fluorescence lifetimes (amplitudes)		Rotational correlation times (amplitudes)	
Proteins	Fraction of population 1	τ_{11} [ns] (α_{11})	τ_{12} [ns] (α_{12})	ϕ_{11} [ns]	τ_{21} [ns] (α_{21})	τ_{22} [ns] (α_{22})	ϕ_{21} [ns] (β_{21})	ϕ_{22} [ns] (β_{22})
Cys3	0.10	2.4 (1.0)	—	1.20	9.3 (0.32)	17.0 (0.68)	1.6 (0.15)	>100 (0.85)
Cys14	0.10	2.2 (1.0)	—	1.0	10.2 (0.25)	18.0 (0.75)	1.7 (0.16)	>100 (0.84)
Cys25	0.08	2.5 (1.0)	—	0.50	10.7 (0.23)	19.0 (0.77)	1.8 (0.15)	>100 (0.85)
Cys36	0.35	7.8 (0.98)	0.30 (0.02)	0.56	10.9 (0.23)	23.0 (0.76)	2.3 (0.12)	53 (0.88)
Cys40	0.33	7.5 (0.50)	0.70 (0.50)	0.48	6.4 (0.40)	27.0 (0.60)	1.8 (0.10)	>100 (0.90)
Cys62	0.31	2.7 (0.80)	0.50 (0.20)	0.57	8.0 (0.30)	22.3 (0.70)	2.3 (0.10)	>100 (0.90)
Cys67	0.30	4.3 (0.61)	0.65 (0.39)	0.48	7.3 (0.30)	22.3 (0.70)	2.1 (0.11)	>100 (0.89)
Cys82	0.30	2.4 (0.52)	0.60 (0.48)	0.45	7.1 (0.34)	24.0 (0.66)	1.0 (0.10)	>100 (0.90)
Cys89	0.33	2.0 (0.50)	0.40 (0.50)	0.30	6.5 (0.56)	21.0 (0.44)	0.9 (0.14)	>100 (0.86)

Fluorescence anisotropy decay measured with the protofibrils formed by the mixture of 2 μM IAEDANS-labeled protein + 48 μM of unlabeled protein was analyzed using Eqs. (5)–(9).
Errors are not mentioned explicitly in order to improve clarity. Errors associated with each measurement are <10%.

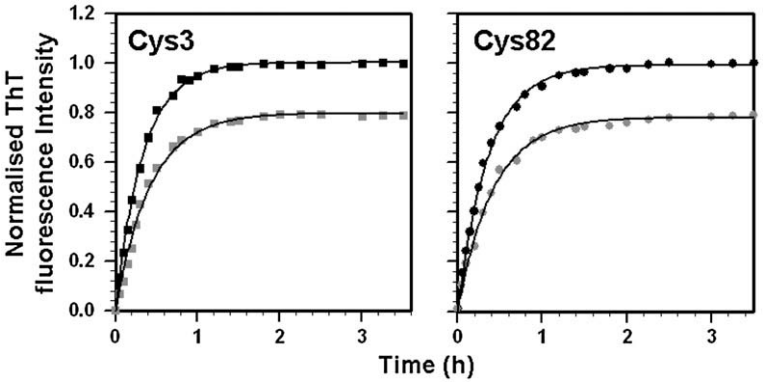

Fig. 5. ThT-monitored kinetics of amyloid protofibril formation by different mutant forms of barstar. Each panel shows the ThT fluorescence monitored kinetics of aggregation of labeled (grey symbols) and unlabeled (black symbols) Cys3 and Cys82. In each case, the protein concentration during the aggregation was 50 μM. Single exponential fits through the data points (continuous lines) yield the following values for the ThT fluorescence-monitored rate constants: 2.95 h^{-1} (unlabeled Cys3), 2.38 h^{-1} (labeled Cys3), 2.74 h^{-1} (unlabeled Cys82), and 2.36 h^{-1} (labeled Cys82).

towards the formation of mixed protofibrils are not surprising as both labeled proteins have different secondary structures. Cys3, which shows a smaller perturbation than does Cys82 upon labeling, can make mixed protofibrils unlike Cys82. Thus, the overall conclusions from the CD spectra indicate that the internal structures of the A-form and the protofibril are altered by labeling of the site directly involved in the ordered aggregation.

Although the internal structure of the polypeptide is altered by IAEDANS labeling, it is important to know whether the macroscopic morphology of the protofibrils is also affected. AFM was used to study the morphologies of the protofibrils formed by the labeled and the unlabeled proteins. Figure 7 shows AFM images of protofibrils formed by Cys3 and Cys82, both labeled and unlabeled, at 50 μM concentration. It appears from Fig. 7a and b that the labeled and unlabeled Cys3 forms protofibrils of similar morphology, which are seen as short, curly, and wormlike aggregates. A similar result is obtained with both labeled and unlabeled Cys82 (Fig. 7c and d). The morphology of the protofibrils appears similar in both the labeled and unlabeled mutant protein forms, and the thickness of the fibrils is also largely unchanged upon labeling. These observations suggest that it is unlikely that fluorescence labeling perturbs the gross morphology of the protofibrils. Thus, it is evident from these experiments that although IAEDANS labeling can perturb the internal secondary structures of the A-form and the protofibrils, the kinetics of formation of proto-

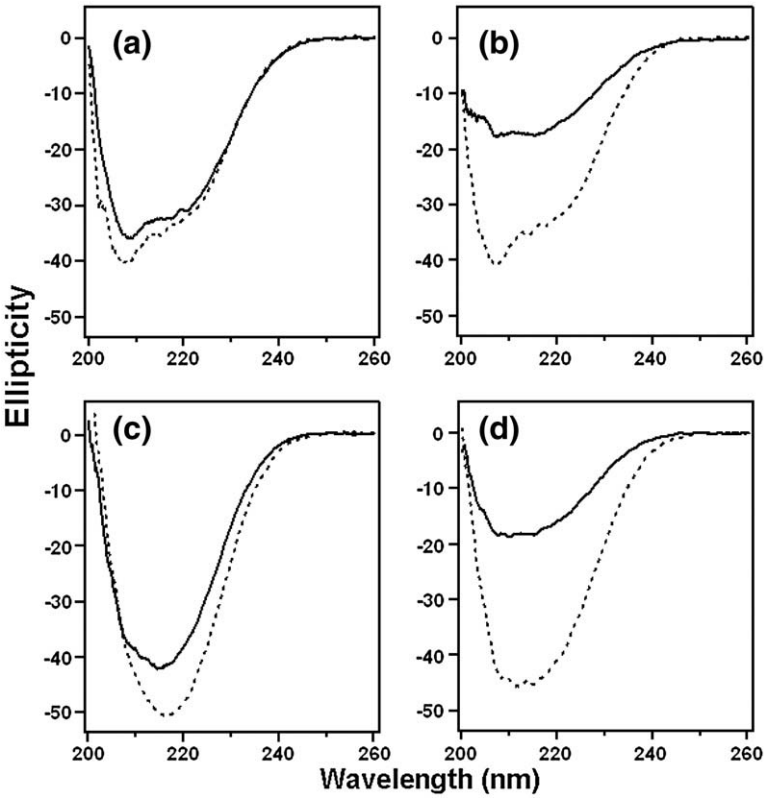

Fig. 6. Far-UV CD spectra show the perturbation in the internal structure of the aggregates due to the IAEDANS labeling. (a) shows the CD spectra of the A-form of Cys3 (broken line) and Cys82 (continuous line). (b) shows the CD spectra of the A-form of Cys3-IAEDANS (broken line) and Cys82-IAEDANS (continuous line). (c) shows the CD spectra of the protofibrils of Cys3 (broken line) and Cys82 (continuous line). (d) shows the CD spectra of the protofibrils of Cys3-IAEDANS (broken line) and Cys82-IAEDANS (continuous line). In each case, the protein concentration during aggregation was 50 μM.

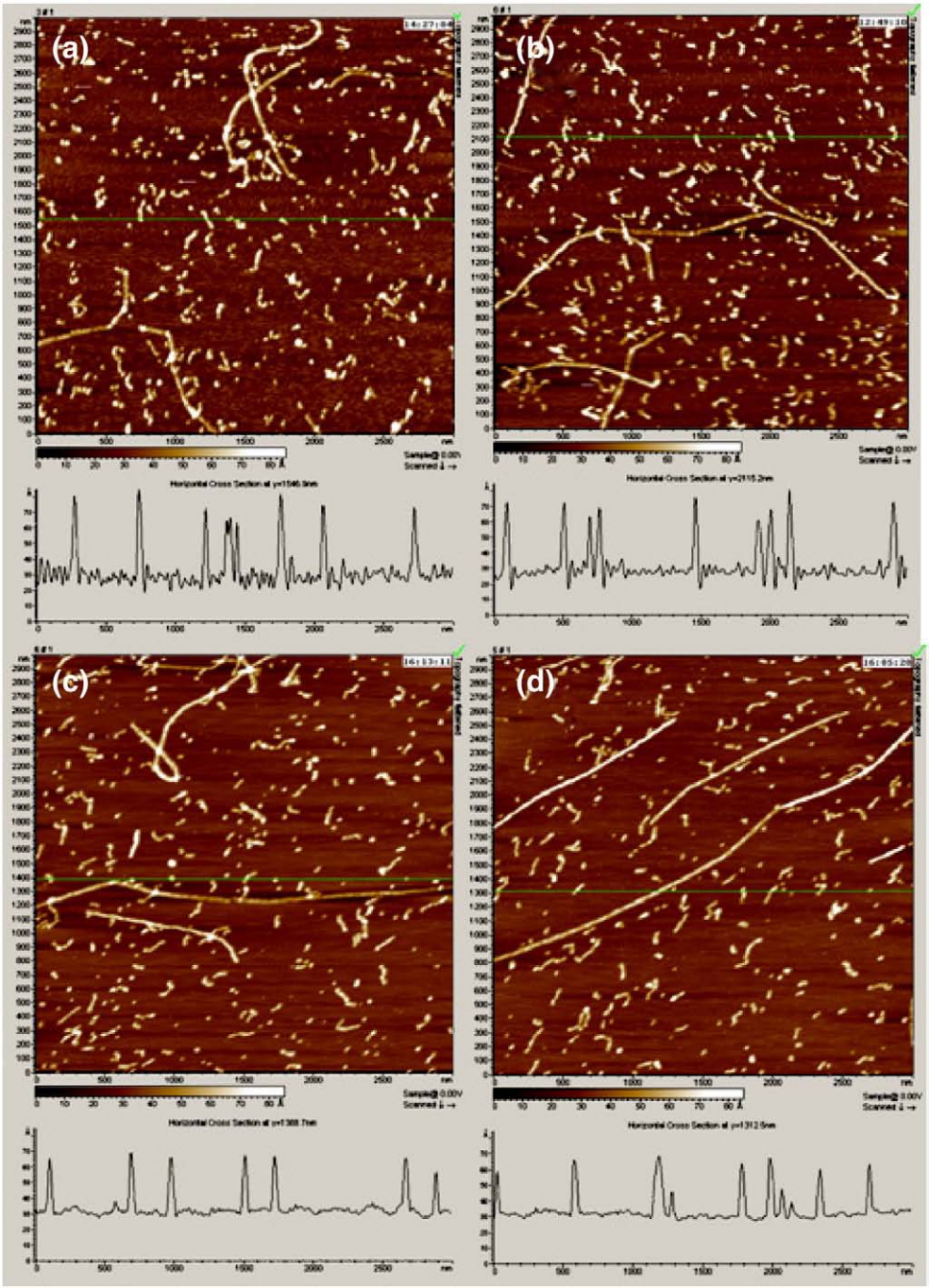

Fig. 7. AFM images (imaged in the dry state) showing the morphology of protofibrils formed by Cys3 and Cys82. (a) and (b) represent the protofibrils formed by labeled and unlabeled Cys3, respectively, at 50 μM concentration. (c) and (d) represent the protofibrils formed by labeled and unlabeled Cys82, respectively, at 50 μM concentration. The bottom part of each panel shows the height along the horizontal green line in the images.

fibrils, as well as the overall external morphology of the protofibrils, are largely unaltered.

Discussion

Self-complimentary interaction in protofibrils

Much is now known about the internal structure of the amyloid fibrils.[46–51] In contrast, very little is known about the internal structure of the protofibrils. Protofibril morphology probed by AFM[34,52,53] and electron micrographs[54] show them as short and curly filamentous structures. AFM imaging studies also appear to indicate that amyloid fibrils form from linear association of protofibril units.[52,55] Site-specific fluorescence spectroscopy is shown here to be a powerful technique for studying the internal structure of protofibrils.

One of the striking observations made in this work is that barstar, when labeled at certain locations with the fluorescent probe 1,5-IAEDANS, does not form co-fibrils with the corresponding unlabeled protein. This conclusion was arrived at by analyzing the population heterogeneity of protein aggregates/fibrils, by exploiting the difference in the hydrodynamic properties of the various species, and by using a fluorophore (1,5-IAEDANS) that has a high level of environment sensitivity. Although a two-population model was used to analyze the data, the incorporation of more than two populations in the model would not affect the conclusion of the work, which is mainly based on the observation of the dip-and-rise pattern in the fluorescence anisotropy decay kinetics.

Furthermore, the labeled proteins were found to form fibrils, and the internal and overall structures of these fibrils were very similar to those of the corresponding unlabeled protein. In contrast, the proteins labeled at some positions do not form mixed protofibrils with the corresponding unlabeled protein. This observation suggests that the internal structure of protofibrils is formed by self-complimentary interactions in a process that may be akin to the process of crystallization, even though the degree of structural order in the protofibrils is likely to be substantially less than seen in the crystals. The similarity between the process of amyloid formation and crystallization is also evident in the observation that both processes involve nucleated growth.[56] The inability of IAEDANS-labeled protein to interact with the corresponding unlabeled protein while forming protofibrils is similar to the inability of molecules having even a minor structural alteration at a specific location to form co-crystals. A recent protein engineering study[57] has brought out the importance of the protein–protein interaction interface in protein self-assembly and of symmetry in the structure. The observation of an inhibitory interaction between Aβ (1–40) and Aβ (1–42), observed in the nucleation process,[58] had earlier suggested the requirement of perfect complimentarity between the interacting partners to form fibrils.

X-ray crystallography studies of amyloid-like fibrils and of the closely related microcrystals formed by amyloidogenic peptides[14,59] reveal a common cross-β spine. In the pair of β-sheets that constitutes the spine, the side chains are tightly interdigitated, resulting in steric zippers that vary with the sequence of the peptide. It is likely that the core of the amyloid protofibrils of barstar is as tightly packed as the core of amyloid fibrils. The interiors of proteins are also very tightly packed,[60,61] and protein engineering studies have shown that the packing interactions in the core are an important determinant of protein stability[62] and that the introduction of cavities in the protein interior is highly destabilizing.[63,64] It is likely that the reason that protein labeled at a core residue in the protofibril does not form mixed fibrils with the corresponding unlabeled mutant protein is that any interaction is destabilized significantly by the absence of the tightly packing interactions. Symmetry probably allows the tight packing and, hence, stabilization of the protofibrils formed by the labeled proteins only or by the unlabeled proteins only.

Identification of regions involved in self-complimentary interaction

The question whether the entire length of a protein is involved in ordered (self-complimentary) interaction has relevance in scoring the propensity of a given sequence to form fibrils. There are indications that amyloid fibrils have some flexible and random segments, apart from a compact and highly ordered core.[14,65–71] The present work addresses this issue for the case of protofibrils and identifies segment(s) that are involved in self-complimentary interactions and those that are not. In the present work on protofibrils from barstar, we infer that residues C3, C14, and C25 are not involved in ordered aggregation, whereas C36, C40, C62, C67, C82, and C89 are intimately involved in self-complimentary interactions in the protofibrils.

It was important to determine whether the inability of C-terminal labeled mutant proteins to form mixed protofibrils with the corresponding unlabeled mutant protein originates in the A-form itself. In order to address this question, we measured fluorescence anisotropy decay kinetics at all the nine locations in the A-form formed by 2 and 50 μM of the labeled proteins and by mixtures of 2 μM of labeled and 48 μM unlabeled mutant proteins. The results of this experiment did not provide a clear picture; that is, while a few of the positions (which showed dip-and-rise in protofibril samples) showed a tendency towards a dip-and-rise behavior, a larger number of locations did not (data not shown). This is not surprising as the differences in the fluorescence lifetimes as well as in the rotational correlation times of various populations in the A-form may not be large, in contrast to the case of protofibrils. Large differences in the fluorescence dynamics parameters are essential to generate a prominent dip-and-rise anisotropy decay.[45] Hence, the observed anisotropy decay data in the A-form does not permit us to answer the question whether co-aggregation occurs in the A-form or not. It should be noted, however, that an NMR study of the structure of A-form of barstar had shown that 20 residues at the N-terminal end of the protein remain flexible, unlike the remainder of the chain that gets packed tightly in the core of the 16-mer aggregate.[29]

The structural information obtained from the present study is of low resolution since it provides discrimination only at the residue level, as to whether the residue is part of the self-complimentary interaction or not. However, such information is important, not only from the perspective for building realistic models but also from the perspective of being able to predict the propensity of a given peptide sequence to form the ordered interactions present in core of the fibrils. The method presented

in this work can be considered as complimentary to other spectroscopic methods such as EPR in identifying ordered and flexible domains.[13] A recent work by solid-state NMR addresses the issue of segregating regions of high and low flexibility in the fibrils of the N-terminal domain of nuclear poly(A) binding protein (PABPN1).[72] The characteristic β-sheet chemical shifts and the order parameters of alanine and glycine residues were used to identify the rigid segments within the fibril.[72]

The power of the method used in this work originates from the high environment sensitivity of the fluorescence probe 1,5-IAEDANS used to label the single cysteine side chain, apart from differences in the hydrodynamic properties of protein aggregates of various sizes. Although differences in these two parameters give rise to the dramatic differences in the anisotropy decay kinetics (Fig. 2 and Table 1), the significant differences in the mean fluorescence lifetimes (Table 2) between samples that form mixed protofibrils and those that do not form them arise only from the environment sensitivity of the fluorophore. Since fluorescence lifetimes are easier to measure than anisotropy decay kinetics, a lifetime-based assay could be envisaged as a general technique to answer the question whether a given site in a sequence is involved in the tight self-complimentary interactions characteristic of the core of protofibrils and fibrils.

What properties of the barstar polypeptide chain give rise to the N-terminal one-third remaining in a non-interacting mode, while the rest of the sequence takes part in self-complimentary interactions? Inspection of the sequence of barstar reveals the presence of six positively charged residues in the first one-third of the sequence. The remaining two-thirds of the chain has only four positively charged side chains. Since all the carboxyls are expected to be protonated and neutral at pH <3, the high prevalence of positive charges in the N-terminal one-third may have caused this segment to remain largely unstructured and flexible.

Figure 8 shows a working model of the structure of protofibrils as inferred from this study. The self-complimentarity of interactions in the rigid core region, inferred from the present work, indicates a parallel organization of strands, as in the case of fibrils formed by the alanine expansion domain.[72] A striking feature of the model presented in Fig. 8 is the involvement of the C-terminal region till its very end, unlike the observations made for several other proteins, where both the N- and C-terminal regions remain flexible, while the interior region forms the ordered core.[13,72] It is stressed, however, that the working model presented in Fig. 8 is derived independently from fluorescence anisotropy and lifetime data. More direct methods of structure determination, for example, solid-state NMR, among others, need to be utilized for verifying the model.

Materials and Methods

Chemicals and buffers

All the chemicals used were of the highest purity grade available from Sigma-Aldrich. 1,5-IAEDANS was from Molecular Probes. The protein was dissolved initially in native buffer (pH 8.0). This was composed of 20 mM Tris–HCl and 250 μM ethylenediaminetetraacetic acid. All the measurements were done at 23 °C.

Protein expression and purification

The *Escherichia coli* strain used for protein expression was MM294. Wild-type barstar has two cysteine residues at positions 40 and 82. All the mutant versions of barstar used in this study contain a single cysteine at one of nine different locations and a single tryptophan (W53). The mutant proteins Cys3, Cys14, Cys25, Cys36, Cys40, Cys62, Cys82, and Cys89 were purified as described previously.[73] Protein purity was checked by mass spectrometry using a Micromass Q-TOF Ultima mass spectrometer coupled with an electrospray ionization source. The purity of each protein was found to be >98%. Protein concentrations

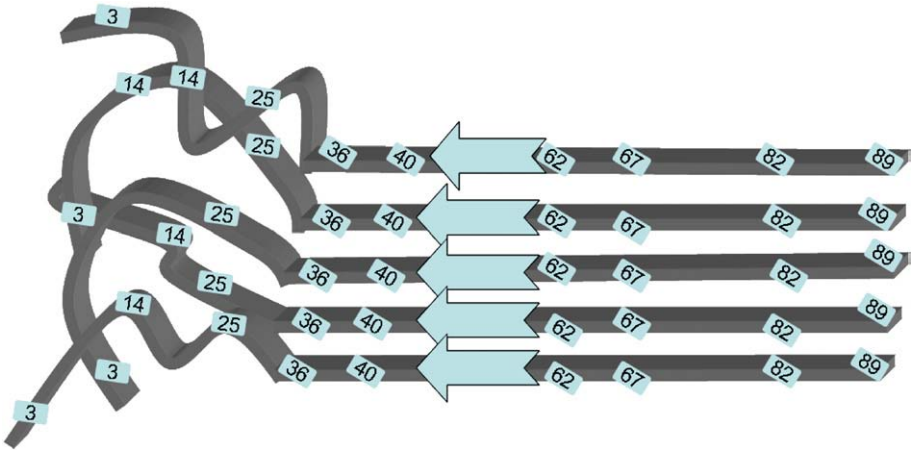

Fig. 8. A schematic working model for the structure of protofibrils. Self-complimentary interactions in the rigid core region point towards a parallel organization of the polypeptide strands. The model shows that the entire C-terminal region, till its very end, participates in the specific interpeptide interactions.

were determined by measuring the absorbance at 280 nm, using an extinction coefficient of 10,000 M^{-1} cm^{-1} for all the mutant proteins.

Preparation of IAEDANS-labeled protein

For time-resolved fluorescence measurements, all the mutant proteins were labeled with the thiol labeling probe 1,5-IAEDANS in 7 M urea and 20 mM Tris–HCl at pH 8, using a 20-fold molar excess of the dye in the dark. This reaction mixture was kept at room temperature for 5 h. After the labeling reaction was complete, the labeled protein was separated from free dye and urea by passing the reaction mixture through a PD-10 column (Pharmacia). The extent of labeling was checked as described earlier[24] and was found to be >95% for all the mutant proteins.

Sample preparation and protofibril formation from native protein

Purified labeled protein was concentrated using a Millipore filter (5 kDa cutoff). A stock solution of 500 μM protein in 20 mM Tris–HCl buffer (pH 8.0) was made. The concentration was checked as described above. The stock solution of the 500 μM labeled native protein was diluted 10-fold into the 50 mM glycine buffer (pH 2.7) to give 50 μM of the A-form. Similarly, a stock solution of the 20 μM labeled native protein was diluted 10-fold into the 50 mM glycine buffer (pH 2.7) to give 2 μM of the A-form. The A-form at both the low and the high concentration was incubated at room temperature for 30 min. The protofibrils were formed by heat (70 °C) treatment for 2.5 h of the A-form in a water bath. The protofibrils were brought back to room temperature after heating and incubated at room temperature for 10–15 min prior to data collection. The mixture of labeled and unlabeled protofibrils was prepared by mixing of the two stock solutions of 480 μM unlabeled and 20 μM labeled protein. This mixture was diluted 10-fold into the 50 mM glycine buffer (pH 2.7) to give the A-form, which was further treated to form protofibrils in a way similar to that described above.

ThT assay

Fluorescence measurements were carried out on a SPEX Fluorolog (T-format) FL111 spectrofluorimeter by exciting the sample at 440 nm and monitoring the fluorescence emission at 482 nm. The excitation and emission slit widths were set at 1 and 7.5 nm, respectively.

A fresh stock solution of 2.52 μM ThT in 35 mM Tris buffer (pH 8.65) was prepared. For the assay, an aliquot of 5 μL of protein (50 μM, in 50 mM glycine buffer, pH 2.7) was taken at different time of heating (70 °C). This aliquot was then added to the 495 μL of the ThT assay solution in 35 mM Tris buffer (pH 8.6) such that the final protein and dye concentrations in the assay solution were 0.5 and 2.5 μM, respectively. The final pH of the assay solution was maintained at 8.0. The sample was mixed thoroughly, and the data were collected within 10–15 s of the addition of ThT to the protein.

Atomic force microscopy

AFM images were obtained on a PicoPlus AFM instrument (Molecular Imaging Inc., Arizona, USA) operating in the non-contact mode. AFM images of both dry and wet samples were taken. AFM cantilevers of the type NCL and PPP-CONT-50 (Nanosensors Inc., Switzerland) were used for the scanning of dry and liquid state images, respectively. The NCL cantilever was used to scan the sample at a frequency of 177 kHz and with a scanning speed of 2.4 lines/s. In contrast, the PPP-CONT-50 cantilever was used at 22 kHz, with a scanning speed of 1.8 lines/s. Dry AFM images were scanned for the protofibrils formed from the 50 μM labeled and unlabeled samples of Cys3 and Cys82. After a 100-fold dilution in 50 mM glycine buffer, pH 2.7, an aliquot of these protofibrils was applied to a freshly cleaved mica surface. After an incubation of 10 s, the mica surface was rinsed five times with 100 μl of water and dried under a mild stream of nitrogen for 35 min before it was scanned. Liquid AFM images were scanned for protofibrils prepared from the 50 and 2 μM labeled samples of Cys82. One microliter of the 50 μM protofibril sample was mixed with 400 μl of 50 mM glycine buffer (pH 2.7) in the liquid cell. For the 2 μM protofibril sample, 25 μl was mixed with 375 μl of 50 mM glycine buffer (pH 2.7) in the liquid cell prior to scanning. Thus, the final concentration of the protein in the liquid cell was kept identical for the two samples.

CD experiment

Protofibrils and the A-form prepared from the 50 μM labeled and unlabeled samples of Cys3 and Cys82 were prepared as described above. Far-UV CD measurements were carried out using a Jasco J-720 spectropolarimeter. The cuvette used for the measurement was of 1 mm path length. Spectra were collected from 200 to 260 nm, with a step resolution of 1 nm, a scan speed of 100 nm/min, and a bandwidth of 1 nm. All the spectra were averaged over five scans.

Time-resolved fluorescence measurements

Time-resolved fluorescence intensity and anisotropy decay kinetics experiments were carried out using a Ti-Sapphire picosecond laser and a time-correlated single-photon counting setup, coupled to a micro-channel plate photomultiplier as described earlier.[20] Pulses of 1 ps duration of 820 nm radiation from the Ti-Sapphire laser were frequency doubled to 410 nm, using a frequency doubler (GWU, Spectra Physics). For all the time-resolved measurements, samples were excited at 410 nm, at a pulse repetition rate of 4 MHz, and emission was measured at 525 nm. The instrument response function (IRF) was obtained at 410 nm, using a very dilute colloidal suspension of dried nondairy coffee whitener. The width (full width at half maximum) of the IRF was ~40 ps. The decay was deconvoluted with respect to the IRF and analyzed using a sum of discrete exponentials as described in Model used and data analysis. For the fluorescence lifetime measurements, peak counts of 10,000 were collected with the emission polarizer oriented at the magic angle (54.7°) with respect to the excitation polarizer. For time-resolved anisotropy measurements, the emission data were collected at 0° (parallel fluorescence intensity $I_{\parallel}$) and 90° (perpendicular fluorescence intensity $I_{\perp}$) with respect to the excitation polarization.

Model used and data analysis

Fluorescence intensity decay curves were analyzed by deconvoluting the observed decay with the IRF to obtain

the intensity decay function represented as a sum of two or three exponentials as

$$I(t) = \sum \alpha_i \exp(-t/\tau_i) \quad i = 2 \text{ or } 3 \tag{1}$$

where $I(t)$ is the fluorescence intensity collected at magic angle (54.7°) at time t and α_i is the amplitudes associated with the fluorescence lifetimes τ_i, such that $\sum \alpha_i = 1$. The mean lifetime $\tau_m = \sum \alpha_i \tau_i$.

The time-resolved fluorescence anisotropy decays were analyzed by globally fitting $I_{||}(t)$ and $I_{\perp}(t)$ as

$$I_{||}(t) = I(t)[1 + 2r(t)]/3 \tag{2}$$

$$I_{\perp}(t) = I(t)[1 - r(t)]/3 \tag{3}$$

where $I_{||}(t)$ and $I_{\perp}(t)$ are the emission intensities collected at polarization directions parallel and perpendicular, respectively, to the polarization of the excitation beam. $r(t)$ is the anisotropy decay function that is modeled in two different ways depending on the situation. For protofibrils formed at high (50 μM) concentration of proteins, it was analyzed as a sum of exponential terms

$$r(t) = r_0 \sum \beta_j \exp\left(-t/\phi_j\right) \quad j = 2 \tag{4}$$

where r_0 is the limiting anisotropy in the absence of rotational diffusion, ϕ_j are the rotational correlation times with amplitudes β_j, such that $\sum \beta_j = 1$. This model assumes a population having uniform fluorescence dynamics properties with each molecule associated with both the correlation times.

In contrast, the anisotropy decay kinetics of protofibrils formed by 2 μM samples as well as mixed samples, which showed a dip-and-rise behavior, could not be fitted with the above model and requires a two-component model. This model assumes the presence of two populations, that is, one being very small aggregates and the other being larger aggregates. Furthermore, the rate of interconversion between the two populations is assumed to be slow when compared to the timescale of fluorescence lifetimes. In this model, each fluorophore population displays its own intensity and anisotropy decay kinetics.[41,42] The time-dependent anisotropy is then given by

$$r(t) = f_1(t) r_1(t) + f_2(t) r_2(t) \tag{5}$$

where $f_1(t)$ and $f_2(t)$ are the fractions of the photons emitted by the very small and larger aggregates at time t, respectively. $r_1(t)$ and $r_2(t)$ are the anisotropy decay functions of the two populations, respectively.

$$r_1(t) = r_0 \exp(-t/\phi_{11}) \tag{6}$$

$$r_2(t) = r_0 \beta_{21} \exp(-t/\phi_{21}) + r_0 \beta_{22} \exp(-t/\phi_{22}) \tag{7}$$

where $\beta_{21} + \beta_{22} = 1$.

The anisotropy decay of the very small oligomers is described by a single rotational correlation time ϕ_{11}. The higher oligomers are described by at least two rotational correlation times, ϕ_{21} and ϕ_{22}, with their amplitudes β_{21} and β_{22}, respectively.

The fractions $f_1(t)$ and $f_2(t)$ are given by

$$f_1(t) = \frac{\alpha_{11}\exp(-t/\tau_{11}) + \alpha_{12}\exp(-t/\tau_{12})}{\alpha_{11}\exp(-t/\tau_{11}) + \alpha_{12}\exp(-t/\tau_{12}) + \alpha_{21}\exp(-t/\tau_{21}) + \alpha_{22}\exp(-t/\tau_{22})} \tag{8}$$

$$f_2(t) = \frac{\alpha_{21}\exp(-t/\tau_{21}) + \alpha_{22}\exp(-t/\tau_{22})}{\alpha_{11}\exp(-t/\tau_{11}) + \alpha_{12}\exp(-t/\tau_{12}) + \alpha_{21}\exp(-t/\tau_{21}) + \alpha_{22}\exp(-t/\tau_{22})} \tag{9}$$

where α_{11} and α_{12} are the relative amplitudes of the fluorescence lifetimes τ_{11} and τ_{12}, respectively, for population 1 (very small oligomers). Similarly, α_{21} and α_{22} are the amplitudes of the fluorescence lifetimes τ_{21} and τ_{22}, respectively, for population 2 (higher oligomers).

While analyzing the anisotropy decay traces by using Eqs. (2)–(9), the parameters associated with the fluorescence intensity decay were kept fixed at the values obtained from the analysis of fluorescence intensity decays collected at the magic angle with respect to the excitation polarization. Furthermore, the initial anisotropy r_0 was also estimated from an independent experiment, in which the decay of the fluorescence anisotropy of the IAEDANS in 70% glycerol was measured and kept fixed at this value while analyzing the anisotropy decay kinetics of the protofibrils. Thus, the number of free parameter gets reduced substantially when the anisotropy decay kinetics are analyzed by using Eqs. (2)–(9). These procedures enhanced the reliability of the estimates of the parameters associated with the anisotropy decay of protofibril samples. The uncertainty in the values of anisotropy decay parameters obtained from this two-step analysis was estimated in several ways as follows: (i) by varying the values of the input (fixed) parameters corresponding to the total emission decay within the range obtained from analysis of the total emission decay, (ii) by analyzing several anisotropy decay kinetic traces obtained for the same sample, and (iii) by analyzing decay kinetics of multiple samples. The goodness of fits were assessed from the values of the reduced χ^2 (1.0–1.2) as well as from the randomness of the residuals.[20]

Acknowledgements

We thank Dr. Samrat Mukhopadhyay for his involvement in the very early part of this work, which led to the first observation of the phenomenon shown in Fig. 2, and Prof. N. Periasamy for the software used in the analysis of time-resolved fluorescence data. We thank M. H. Kombrabail for assistance with the AFM measurements. J.B.U. is the recipient of a J. C. Bose National Research Fellowship from the Government of India. This work was funded by the Tata Institute of Fundamental Research and by the Department of Biotechnology and the Department of Science and Technology, Government of India.

References

1. Zerovnik, E. (2002). Amyloid-fibril formation. Proposed mechanisms and relevance to conformational disease. *Eur. J. Biochem.* **269**, 3362–3371.
2. Cohen, F. E. & Kelly, J. W. (2003). Therapeutic approaches to protein-misfolding diseases. *Nature*, **426**, 905–909.
3. Selkoe, D. J. (2003). Folding proteins in fatal ways. *Nature*, **426**, 900–904.

4. Masliah, E. (2008). Alzheimer's in real time. *Nature*, **451**, 638–639.
5. Chiti, F. & Dobson, C. M. (2009). Amyloid formation by globular proteins under native conditions. *Nat. Chem. Biol.* **5**, 15–22.
6. Makin, O. S. & Serpell, L. C. (2004). Structural characterization of islet amyloid polypeptide fibrils. *J. Mol. Biol.* **335**, 1279–1288.
7. Lambert, M. P., Barlow, A. K., Chromy, B. A., Edwards, C., Freed, R., Liosatos, M. *et al.* (1998). Diffusible, nonfibrillar ligands derived from $A\beta_{1-42}$ are potent central nervous system neurotoxins. *Proc. Natl Acad. Sci. USA*, **95**, 6448–6453.
8. Bucciantini, M., Giannoni, E., Chiti, F., Baroni, F., Formigli, L., Zurdo, J. *et al.* (2002). Inherent toxicity of aggregates implies a common mechanism for protein misfolding diseases. *Nature*, **416**, 507–511.
9. Kayed, R., Head, E., Thompson, J. L., McIntire, T. M., Milton, S. C., Cotman, C. W. & Glabe, C. G. (2003). Common structure of soluble amyloid oligomers implies common mechanism of pathogenesis. *Science*, **300**, 486–489.
10. Caughey, B. & Lansbury, P. T. (2003). Protofibrils, pores, fibrils, and neurodegeneration: separating the responsible protein aggregates from the innocent bystanders. *Annu. Rev. Neurosci.* **26**, 267–298.
11. Balbirnie, M., Grothe, R. & Eisenberg, D. S. (2001). An amyloid-forming peptide from the yeast prion Sup35 reveals a dehydrated β-sheet structure for amyloid. *Proc. Natl Acad. Sci. USA*, **98**, 2375–2380.
12. Petkova, A. T., Ishii, Y., Balbach, J. J., Antzutkin, O. N., Leapman, R. D., Delaglio, F. & Tycko, R. (2002). A structural model for Alzheimer's β-amyloid fibrils based on experimental constraints from solid state NMR. *Proc. Natl Acad. Sci. USA*, **99**, 16742–16747.
13. Torok, M., Milton, S., Kayed, R., Wu, P., McIntire, T., Glabe, C. G. & Langen, R. (2002). Structural and dynamic features of Alzheimer's Aβ peptide in amyloid fibrils studied by site-directed spin labeling. *J. Biol. Chem.* **277**, 40810–40815.
14. Sawaya, M. R., Sambashivan, S., Nelson, R., Ivanova, M. I., Sievers, S. A., Apostol, M. I. *et al.* (2007). Atomic structures of amyloid cross-β spines reveal varied steric zippers. *Nature*, **447**, 453–457.
15. Vilar, M., Chou, H., Luhrs, T., Maji, S. K., Riek-Loher, D. & Verel, R. (2008). The fold of α-synuclein fibrils. *Proc. Natl Acad. Sci. USA*, **105**, 8637–8642.
16. Allsop, D., Swanson, L., Moore, S., Davies, Y., York, A., El-Agnaf, O. M. A. & Soutar, I. (2001). Fluorescence anisotropy: a method for early detection of Alzheimer β-peptide (Aβ) aggregation. *Biochem. Biophys. Res. Commun.* **285**, 58–63.
17. Padrick, S. B. & Miranker, A. D. (2002). Islet amyloid: phase partitioning and secondary nucleation are central to the mechanism of fibrillogenesis. *Biochemistry*, **41**, 4694–4703.
18. Krishnan, R. & Lindquist, S. L. (2005). Structural insights into a yeast prion illuminate nucleation and strain diversity. *Nature*, **435**, 765–772.
19. Koo, B. W. & Miranker, A. D. (2005). Contribution of the intrinsic disulfide to the assembly mechanism of islet amyloid. *Protein Sci.* **14**, 231–239.
20. Mukhopadhyay, S., Nayak, P. K., Udgaonkar, J. B. & Krishnamoorthy, G. (2006). Characterization of the formation of amyloid protofibrils from barstar by mapping residue-specific fluorescence dynamics. *J. Mol. Biol.* **358**, 935–942.
21. Dobson, C. M. (2002). Getting out of shape. *Nature*, **418**, 729–730.
22. Stefani, M. & Dobson, C. M. (2003). Protein aggregation and aggregate toxicity: new insights into protein folding, misfolding diseases and biological evolution. *J. Mol. Med.* **81**, 678–699.
23. Uversky, V. N. & Fink, A. L. (2004). Conformational constraints for amyloid fibrillation: the importance of being unfolded. *Biochim. Biophys. Acta*, **1698**, 131–153.
24. Saxena, A. M., Udgaonkar, J. B. & Krishnamoorthy, G. (2006). Characterization of intra-molecular distances and site-specific dynamics in chemically unfolded barstar: evidence for denaturant-dependent non-random structure. *J. Mol. Biol.* **359**, 174–189.
25. Jha, S. K. & Udgaonkar, J. B. (2007). Exploring the cooperativity of the fast folding reaction of a small protein using pulsed thiol labeling and mass spectrometry. *J. Biol. Chem.* **282**, 37479–37491.
26. Pradeep, L. & Udgaonkar, J. B. (2007). Diffusional barrier in the unfolding of a small protein. *J. Mol. Biol.* **366**, 1016–1028.
27. Sinha, K. K. & Udgaonkar, J. B. (2007). Dissecting the non-specific and specific components of the initial folding reaction of barstar by multi-site FRET measurements. *J. Mol. Biol.* **370**, 385–405.
28. Lubienski, M. J., Bycroft, M., Freund, S. M. V. & Fersht, A. R. (1994). 3-Dimensional solution structure and ^{13}C assignments of barstar using nuclear magnetic resonance spectroscopy. *Biochemistry*, **33**, 8866–8877.
29. Juneja, J., Bhavesh, N. S., Udgaonkar, J. B. & Hosur, R. V. (2002). NMR identification and characterization of the flexible regions in the 160 kDa molten globule-like aggregate of barstar at low pH. *Biochemistry*, **41**, 9885–9899.
30. Swaminathan, R., Periasamy, N., Udgaonkar, J. B. & Krishnamoorthy, G. (1994). Molten globule-like conformation of barstar: a study by fluorescence dynamics. *J. Phys. Chem.* **98**, 9270–9278.
31. Khurana, R., Hate, A. T., Nath, U. & Udgaonkar, J. B. (1995). pH dependence of the stability of barstar to chemical and thermal denaturation. *Protein Sci.* **4**, 1133–1144.
32. Kumar, S., Mohanty, S. K. & Udgaonkar, J. B. (2007). Mechanism of formation of amyloid protofibrils of barstar from soluble oligomers: evidence for multiple steps and lateral association coupled to conformational conversion. *J. Mol. Biol.* **367**, 1186–1204.
33. Gast, K., Modler, A. J., Damaschun, H., Krober, R., Lutsch, G., Zirwer, D. *et al.* (2003). Effect of environmental conditions on aggregation and fibril formation of barstar. *Eur. Biophys. J.* **32**, 710–723.
34. Kumar, S. & Udgaonkar, J. B. (2009). Conformational conversion may precede or follow aggregate elongation on alternative pathways of amyloid protofibril formation. *J. Mol. Biol.* **385**, 1266–1276.
35. Jha, A., Udgaonkar, J. B. & Krishnamoorthy, G. (2008). Towards elucidating the internal structure of protein protofibrils: site-specific fluorescence anisotropy decay kinetics. *Proceedings of Trombay Symposium on Radiation and Photochemistry*, pp. 307–308.
36. Goldsbury, C., Kistler, J., Aebi, U., Arvinte, T. & Cooper, G. J. (1999). Watching amyloid fibrils grow by time-lapse atomic force microscopy. *J. Mol. Biol.* **285**, 33–39.
37. Bauer, H., Aebi, U., Haener, M., Hermann, R., Mueller, M., Arvinte, T. & Merkle, H. P. (1995). Architecture and polymorphism of fibrillar supramolecular assemblies produced by in vitro aggregation of human calcitonin. *J. Struct. Biol.* **115**, 1–15.

38. Goldsbury, C. S., Cooper, G. J. S., Goldie, K. N., Muller, S. A., Engel, A., Aebi, U. & Kistler, J. (1997). Polymorphic fibrillar assembly of human amylin. *J. Struct. Biol.* **119**, 17–27.
39. Thirunavukkuarasu, S., Jares-Erijman, E. A. & Jovin, T. M. (2008). Multiparametric fluorescence detection of early stages in the amyloid protein aggregation of pyrene-labeled α-synuclein. *J. Mol. Biol.* **378**, 1064–1073.
40. Carver, T. E., Jr., Hochstrasser, R. A. & Millar, D. P. (1994). Proofreading DNA: recognition of aberrant DNA termini by the Klenow fragment of DNA polymerase I. *Proc. Natl Acad. Sci. USA*, **91**, 10670–10674.
41. Srivastava, A. & Krishnamoorthy, G. (1997). Cell type and spatial location dependence of cytoplasmic viscosity measured by time-resolved fluorescence microscopy. *Arch. Biochem. Biophys.* **340**, 159–167.
42. Lakowicz, J. R. (2006). *Principles of Fluorescence Spectroscopy*, 3rd edit. Kluwer Academic/Plenum Publishers, New York, NY.
43. Bailey, M. F., Thompson, E. H. & Millar, D. P. (2001). Probing DNA polymerase fidelity mechanisms using time-resolved fluorescence anisotropy. *Methods*, **25**, 62–77.
44. Rami, B. R., Krishnamoorthy, G. & Udgaonkar, J. B. (2003). Dynamics of the core tryptophan during the formation of a productive molten globule intermediate of barstar. *Biochemistry*, **42**, 7986–8000.
45. Ludescher, R. D., Peting, L., Hudson, S. & Hudson, B. (1987). Time-resolved fluorescence anisotropy for systems with lifetime and dynamic heterogeneity. *Biophys. Chem.* **28**, 59–75.
46. Diaz-Avalos, R., Long, C., Fontano, E., Balbirnie, M., Grothe, R., Eisenberg, D. & Caspar, D. L. (2003). Cross-β order and diversity in nanocrystals of an amyloid-forming peptide. *J. Mol. Biol.* **330**, 1165–1175.
47. Makin, O. S., Atkins, E., Sikorski, P., Johansson, J. & Serpell, L. C. (2005). Molecular basis for amyloid fibril formation and stability. *Proc. Natl Acad. Sci. USA*, **102**, 315–320.
48. Iwata, K., Fujiwara, T., Matsuki, Y., Akutsu, H., Takahashi, S., Naiki, H. & Goto, Y. (2006). 3D structure of amyloid protofilaments of β_2-microglobulin fragment probed by solid-state NMR. *Proc. Natl Acad. Sci. USA*, **103**, 18119–18124.
49. Tycko, R. (2006). Solid-state NMR as a probe of amyloid structure. *Protein Pept. Lett.* **13**, 229–234.
50. Chen, M., Margittai, M., Chen, J. & Langen, R. (2007). Investigation of α-synuclein fibril structure by site-directed spin labeling. *J. Biol. Chem.* **282**, 24970–24979.
51. Van der Wel, P. C. A., Lewandowski, J. R. & Griffin, R. G. (2007). Solid-state NMR study of amyloid nanocrystals and fibrils formed by the peptide GNNQQNY from yeast prion protein Sup35p. *J. Am. Chem. Soc.* **129**, 5117–5130.
52. Harper, J. D., Wong, S. S., Lieber, C. M. & Lansbury, P. T., Jr (1999). Assembly of Aβ amyloid protofibrils: an in vitro model for a possible early event in Alzheimer's disease. *Biochemistry*, **38**, 8972–8980.
53. Conway, K. A., Lee, S. J., Rochet, J. C., Ding, T. T., Williamson, R. E. & Lansbury, P. T., Jr (2000). Acceleration of oligomerization, not fibrillization, is a shared property of both α-synuclein mutations linked to early-onset Parkinson's disease: implications for pathogenesis and therapy. *Proc. Natl Acad. Sci. USA*, **97**, 571–576.
54. Fowler, W. E., Hantgan, R. R., Hermans, J. & Erickson, H. P. (1981). Structure of the fibrin protofibril. *Proc. Natl Acad. Sci. USA*, **78**, 4872–4876.
55. Harper, J. D., Lieber, C. M. & Lansbury, P. T., Jr. (1997). Atomic force microscopic imaging of seeded fibril formation and fibril branching by the Alzheimer's disease amyloid-beta protein. *Chem. Biol.* **4**, 951–959.
56. Jarrett, J. T. & Lansbury, P. T., Jr. (1992). Amyloid fibril formation requires a chemically discriminating nucleation event: studies of an amyloidogenic sequence from the bacterial protein OsmB. *Biochemistry*, **31**, 12345–12352.
57. Grueninger, D., Treiber, N., Ziegler, M. O., Koetter, J. W., Schulze, M. S. & Schulz, G. E. (2008). Designed protein–protein association. *Science*, **319**, 206–209.
58. Hasegawa, K., Yamaguchi, I., Omata, S., Gejyo, F. & Naiki, H. (1999). Interaction between Aβ(1–42) and Aβ(1–40) in Alzheimer's β-amyloid fibril formation in vitro. *Biochemistry*, **38**, 15514–15521.
59. Nelson, R., Sawaya, M. R., Balbirnie, M., Madsen, A. Ø., Riekel, C., Grothe, R. & Eisenberg, D. (2005). Structure of the cross-β spine of amyloid-like fibrils. *Nature*, **435**, 773–778.
60. Chothia, C. (1975). Structural invariants in protein folding. *Nature*, **254**, 304–308.
61. Richards, F. M. (1977). Areas, volumes, packing and protein structure. *Annu. Rev. Biophys. Bioeng.* **6**, 151–176.
62. Lim, W. A. & Sauer, R. T. (1989). Alternative packing arrangements in the hydrophobic core of lambda repressor. *Nature*, **339**, 31–36.
63. Eriksson, A. E., Baase, W. A., Zhang, X. J., Heinz, D. W., Blaber, M., Baldwin, E. P. & Matthews, B. W. (1992). Response of a protein structure to cavity-creating mutations and its relation to the hydrophobic effect. *Science*, **255**, 178–183.
64. Lee, B. (1993). Estimation of the maximum change in stability of globular proteins upon mutation of a hydrophobic residue to another of smaller size. *Protein Sci.* **2**, 733–738.
65. Jimenez, J. L., Guijarro, J. I., Orlova, E., Zurdo, J., Dobson, C. M., Sunde, M. & Saibil, H. R. (1999). Cryo-electron microscopy structure of an SH3 amyloid fibril and model of the molecular packing. *EMBO J.* **18**, 815–821.
66. Kheterpal, I., Williams, A., Murphy, C., Bledsoe, B. & Wetzel, R. (2001). Structural features of the Aβ amyloid fibril elucidated by limited proteolysis. *Biochemistry*, **40**, 11757–11767.
67. Jimenez, J. L., Nettleton, E. J., Bouchard, M., Robinson, C. V., Dobson, C. M. & Saibil, H. R. (2002). The protofilament structure of insulin amyloid fibrils. *Proc. Natl Acad. Sci. USA*, **99**, 9196–9201.
68. Miake, H., Mizusawa, H., Iwatsubo, T. & Hasegawa, M. (2002). Biochemical characterization of the core structure of α-synuclein filaments. *J. Biol. Chem.* **277**, 19213–19219.
69. Ivanova, M. I., Sawaya, M. R., Gingery, M., Attinger, A. & Eisenberg, D. (2004). An amyloid-forming segment of β_2-microglobulin suggests a molecular model for the fibril. *Proc. Natl Acad. Sci. USA*, **101**, 10584–10589.
70. Kajava, A. V., Baxa, U., Wickner, R. B. & Steven, A. C. (2004). A model for Ure2p prion filaments and other amyloids: the parallel superplated β-structure. *Proc. Natl Acad. Sci. USA*, **101**, 7885–7890.

71. Tycko, R. (2004). Progress towards a molecular-level structural understanding of amyloid fibrils. *Curr. Opin. Struct. Biol.* **14**, 96–103.
72. Sackewitz, M., Scheidt, H. A., Lodderstedt, G., Schierhorn, A., Schwarz, E. & Huster, D. (2008). Structural and dynamical characterization of fibrils from a disease-associated alanine expansion domain using proteolysis and solid-state NMR spectroscopy. *J. Am. Chem. Soc.* **130**, 7172–7173.
73. Sridevi, K. & Udgaonkar, J. B. (2003). Surface expansion is independent of and occurs faster than core solvation during the unfolding of barstar. *Biochemistry*, **42**, 1551–1563.